Gas Separations in Hollow-Fiber Adsorbers

Gary L. Gilleskie, Jennifer L. Parker, and E. L. Cussler

Chemical Engineering and Materials Science, University of Minnesota, Minneapolis, MN 55455

The adsorption of ethane from helium was measured in beds packed with 2.5 μm zeolite crystals and containing either a single hollow fiber or multiple fibers. The single-fiber experiments indicate that the mass-transfer rate in beds containing zeolite 13X is limited by diffusion across the fiber wall and through macropores. For adsorption in single-fiber beds packed with zeolite 4A, mass transfer is limited by micropore diffusion within the particles. Breakthrough curves from beds containing 13X are adequately described with the linear driving force model, while curves from beds containing 4A are consistent with the Rosen model.

Breakthrough curves from beds packed with zeolite 13X and containing multiple fibers can be predicted from the experiments with single-fiber beds when the fibers are evenly spaced. When fibers are unevenly spaced, the breakthrough curves are more disperse. Unevenly spaced fibers are the normal case. Even when fibers are evenly spaced, the productivity of hollow-fiber beds is expected to be no greater than that in conventional beds.

Introduction

Most adsorption processes depend on packed beds, long columns filled with stationary, roughly spherical adsorbent particles. When a gas mixture is pumped into one end of the bed, one species can be preferentially adsorbed. As this gas mixture continues to be the fed, the exiting gas is depleted in this more strongly adsorbed species. Finally, when the adsorbent is almost saturated, the strongly adsorbed species "breaks through" the bed, rising abruptly to approach the feed concentration. A record of the effluent concentration, called a "breakthrough curve," reflects the chemistry and transport in the bed, including the equilibrium uptake and the mass transfer.

Adsorption in packed beds is an effective separation process, the basis of gas separations like pressure swing adsorption. The method often works well. In some cases, however, the performance of the packed beds is compromised by excessive pressure drop, by particle attrition, and by polydispersity in particle size. These compromises can cause breakthrough curves that are more gradual, rather than sharp steps. They can cause breakthrough curves that become less sharp with bed use.

This article experimentally investigates the use of hollow-fiber beds for gas adsorption. These beds should show lower pressure drops, less attrition, and smaller polydispersity. Be-

fore describing our experiments, we can estimate the magnitude of the improvements that we might hope to obtain. To illustrate the lower pressure drop, we consider a gas flowing at the same superficial velocity through a hollow fiber bed and a conventional packed bed (Gibbs and Lightfoot, 1986). In a hollow fiber, the pressure drop Δp and superficial velocity v_0 are related by the Hagen-Poiseuille equation (Bird et al., 1960):

$$\frac{\Delta p}{L}\text{(fiber bed)} = \frac{v_0}{\epsilon}\left(\frac{32\mu}{d^2}\right) \qquad (1)$$

where L is the length of the bed, μ is the gas viscosity, ϵ is the lumen volume per bed volume, and d is the inner diameter of the fiber. The pressure drop in a conventional packed bed is given by the Blake-Kozeny equation (Bird et al., 1960):

$$\frac{\Delta p}{L'}\text{(packed bed)} = v_0'\left(\frac{(1-\epsilon')^2 150\mu}{(\epsilon')^3(d')^2}\right) \qquad (2)$$

where v_0' is the superficial velocity in the bed and d' is the particle diameter. If the fiber diameter and particle diameter

are equal, and if $\epsilon = \epsilon' = 0.4$, then the ratio of the pressure drop in the fiber bed to that in the conventional bed at equal gas velocities is given by

$$\frac{\Delta p/L(\text{fiber bed})}{\Delta p/L'(\text{packed bed})} = \frac{32}{150} \frac{\epsilon'^2}{(1-\epsilon')^2} \frac{(d')^2}{d^2} = 0.095. \quad (3)$$

This ratio shows that when the particle diameter and hollow-fiber diameter are equal, the fiber beds produce a smaller pressure drop. For this ratio to be closer to unity, the particle diameter must be bigger than the fiber diameter. Mass-transfer rates, however, are often limited by particle diffusion (Garg and Ruthven, 1973); therefore, an increase in particle diameter may compromise bed performance. The pressure drop in a fiber bed depends only on the fiber diameter and not the thickness of adsorbent surrounding the fiber, so the pressure drop may be minimized without altering bed dynamics. Thus hollow-fiber beds may find special value in applications requiring small pressure drops.

A second potential advantage offered by the hollow-fiber system is the reduction in particle attrition. Attrition comes from the abrasion that may take place between particles when beds become fluidized. Fluidization can occur when significant drag forces caused by high pressure drops are present in the bed. Attrition has been identified as a significant problem in both traditional pressure swing adsorption and rapid pressure swing adsorption processes (Turnock and Kadlec, 1971; White and Barkley, 1989). The frequency and severity of attrition prompted the Pall Corporation to develop techniques for immobilizing particles within packed beds. The methods developed, described in a series of patents (Degen and Gsell, 1987a,b; Miller and Verrando, 1987) anchor absorbent particles to a polymeric binding material. Fiber beds may make this unnecessary.

The third potential advantage of hollow-fiber beds is the monodisperse diameter of the hollow fibers. These diameters are routinely constant within 2%, which is significantly more uniform than the diameters of particles in conventional packed beds. On reflection, we realize that this advantage may be illusory: the altered flow allowed by a big fiber will be felt over the entire length of the bed, but the altered flow engendered by a big particle will decay after perhaps ten particle diameters. We are not sure how much gain can come from monodisperse fibers.

Interestingly, others have suggested adsorption in geometries similar to a hollow fiber bed. For example, Sartory (1978) and Tereck et al. (1987) present theories for adsorption from a feed into a thin coating on the walls of a cylindrical channel. Sartory wanted to use this geometry for clinical purposes. Tereck et al. sought better physical models for packed beds. In both cases, no attempt was made to test the geometry experimentally. While the thin coating of adsorbent would not normally provide the capacity needed for any bulk separation, a recent patent hints at advantages for these hollow-fiber geometries, but gives few details (McMinis and Pan, 1992).

In this article, we report results from our measurements of breakthrough curves for beds containing only a single fiber and for beds containing multiple fibers. We begin this article with a discussion of two models appropriate for analyzing
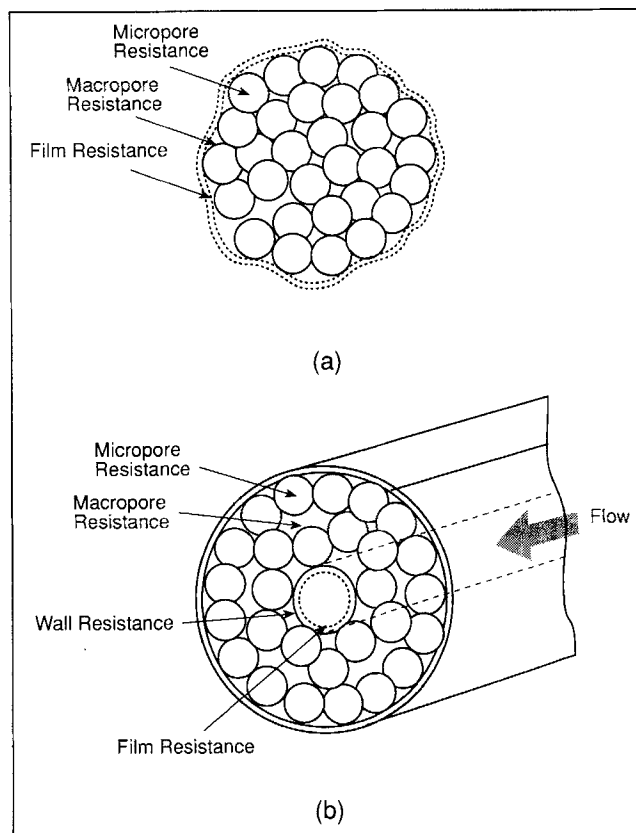

Figure 1. Mass transfer in a conventional bed vs. in a hollow fiber bed.

The mass-transfer transfer resistances in and around a zeolite pellet made of many crystals are similar to the resistances associated with a single hollow fiber passing through a bed of zeolite crystals.

breakthrough behavior in hollow fiber beds. We then describe our experiments with these beds as well as our results from these experiments. Finally, we compare the performance of hollow-fiber and conventional beds.

Theory

In this section, we adapt existing breakthrough models to our hollow-fiber beds. In some ways, the shell side of our hollow-fiber bed, containing very small zeolite crystals, is similar to one very large pellet made by binding very small crystals together. In both cases, gas must diffuse through macropores into the crystal micropores in order to be adsorbed. The mass transfer in such a hollow-fiber bed is compared in Figure 1 with that in a pellet.

Like the conventional pellet, a hollow-fiber bed contains a film resistance, a macropore resistance, and a micropore resistance. Unlike the conventional pellet, the hollow-fiber bed contains a resistance due to the hollow-fiber wall. Determining how these resistances affect the dynamics of hollow-fiber beds is one goal of this article.

Two breakthrough models typically used for conventional packed beds are easily adapted for use with hollow-fiber beds: the linear driving force model (Anzelius, 1926; Ruthven, 1984) and the Rosen model (Rosen, 1952, 1954). The models differ

in the form of the expression used to describe mass-transfer rates. To show how these models differ, we begin with the fluid phase mass balance over a differential section of hollow-fiber bed through which a gas mixture containing a trace amount of a single adsorbable species is flowing:

$$v_0 \frac{\partial c}{\partial z} + \epsilon \frac{\partial c}{\partial t} + \alpha \frac{\partial \bar{\bar{q}}}{\partial t} = 0 \qquad (4)$$

where c is the concentration of solute in the gas phase within the fiber lumen, and $\bar{\bar{q}}$ is the concentration of adsorbed solute averaged over the volume of particles in the differential section. The porosity ϵ is the fraction of column volume that is available for flow (the volume fraction occupied by the inner diameter of the fibers), and α is the fraction of column volume occupied by particles. Because there are voids in the shell side of the module and because the hollow-fiber wall has a finite thickness, the sum of ϵ and α is less than one. Equation 4 implies negligible axial dispersion, constant velocity through the hollow fiber, and negligible accumulation of solute in the macropores of the shell side.

For the case in which an initially clean column is subjected to a step change in the solute concentration at the column inlet, the appropriate initial and boundary conditions are

$$\bar{\bar{q}}(0, z) = c(0, z) = 0 \qquad (5)$$

$$c(t, 0) = c_0. \qquad (6)$$

The concentration q^* of the solute in the solid phase that would be in equilibrium with the gas phase is assumed to be

$$q^* = Kc \qquad (7)$$

where K is an equilibrium constant.

As mentioned earlier, the linear driving force model and the Rosen model differ in the expression used to describe mass-transfer rates. First, we consider the linear driving force model. As the name implies, this model assumes

$$\frac{\partial \bar{\bar{q}}}{\partial t} = k(q^* - \bar{\bar{q}}) \qquad (8)$$

where k is a rate constant with the dimensions of reciprocal time. The solution of Eqs. 4-8 is

$$\frac{c}{c_0} = \exp(-\xi_L) \int_0^{\tau_L} \exp(-u) I_0\left(2\sqrt{\xi_L u}\right) du$$

$$+ \exp(-\xi_L - \tau_L) I_0\left(2\sqrt{\xi_L \tau_L}\right) \quad (9)$$

where the dimensionless distance is

$$\xi_L = \frac{kKz\alpha}{v_0} \qquad (10)$$

and the dimensionless time is

$$\tau_L = k(t - \epsilon z/v_0). \qquad (11)$$

This model will be most useful in cases where mass transfer is slow outside of the adsorbent particles.

The rate constant k that appears in Eqs. 8-11 is given by

$$\frac{1}{k} = \frac{K}{k_{\text{lumen}}a} + \frac{K}{k_{\text{wall}}a} + \frac{1}{k'} \qquad (12)$$

where k_{lumen}, k_{wall}, and k' are the mass-transfer coefficients in the hollow-fiber lumen, the hollow fiber wall, and the macropores and micropores, respectively, and a is the fiber area per volume of adsorbent particles. We know of no expression to account for the resistance due to macropore diffusion and hence will consider it as an unknown parameter in our experiments.

We can use past studies to estimate the individual mass-transfer coefficients in Eq. 12. For mass transfer within the lumen,

$$k_{\text{lumen}} = 4.364 \frac{D}{d} \qquad (13)$$

where D is the diffusion coefficient of the solute in the bulk solvent gas (Newman, 1969; Tereck et al., 1987). This result implies a small Graetz number, which is the case for our experiments. For mass transfer across the hollow-fiber membrane wall,

$$k_{\text{wall}} = \frac{D_{\text{wall}}\theta}{\delta} \qquad (14)$$

where D_{wall} is the diffusion coefficient of the gas through the membrane pores, θ is the porosity of the hollow-fiber wall, and δ is the effective wall thickness including the tortuosity (Qi and Cussler, 1985). Values for θ can usually be obtained from the membrane manufacturer, but values for D_{wall} and δ must be estimated.

Values for the mass-transfer coefficients associated with macropore and micropore diffusion are more difficult to estimate. As mentioned, we know of no way to guess the resistance in the macropores, so we must treat the mass-transfer coefficient k' for this step as unknown. We have several alternatives. One possibility is to use the approximation that the micropores dominate, so

$$k' = k_{\text{micro}} = \frac{60 D_{\text{micro}}}{(d')^2} \qquad (15)$$

where D_{micro} is the effective diffusion coefficient of the adsorbate in the particle and d' is again the particle diameter. This expression, originally derived by Glueckauf (1955), uses the well-known solution for the time change in the average concentration of an adsorbate in an initially clean particle whose surface is suddenly exposed to a constant concentration of the adsorbate (Carslaw and Jaeger, 1947). The expression has been used to model mass-transfer rates in a variety of linear adsorption processes; however, the expression is strictly valid only when the adsorption isotherm is linear and when the dimensionless ratio $4D_{\text{micro}}t/(d')^2$ has a value greater than 0.1. While the derivation of Eq. 15 assumes a spherical particle, it is often applied to other geometries.

An alternative to the linear driving force model is the Rosen model, which focuses on what happens within the particles. In more quantitative terms, the linear driving force model cannot accurately account for intracrystalline mass transfer for cases in which $4D_{micro}t/(d')^2 < 0.1$. In order for this dimensionless ratio to have a value greater than 0.1, D_{micro} must be relatively large; therefore the linear driving force model will usually not be accurate under conditions of micropore control.

The Rosen model assumes that diffusion into the particle limits mass transfer and hence is applicable to beds operating under micropore diffusion control. In this case, solute transport within the fiber, across the fiber wall, and within the macropores of the shell side is sufficiently rapid to maintain a concentration in the macropores that is equal to the concentration of solute flowing through the fiber. Under these conditions, the gas-phase concentration of solute at a particular value of z is independent of the radial position in the column. The rate of solute transport from the fiber lumen into the adsorbent is given by

$$\frac{\partial q}{\partial t} = \frac{1}{r^2}\frac{\partial}{\partial r}\left(D_{micro}r^2\frac{\partial q}{\partial r}\right), \qquad (16)$$

which is subject to

$$q(t, r = d'/2) = Kc \qquad (17)$$

$$\frac{\partial q}{\partial r}(t,0) = 0 \qquad (18)$$

$$\bar{\bar{q}} = \bar{q} = \frac{3}{(d'/2)}\int_0^{d'/2} qr^2\,dr. \qquad (19)$$

The solute concentrations q, $\bar{q}$, and $\bar{\bar{q}}$ are within the crystal, averaged over a particle, and averaged over the bed, respectively. Equation 16 applies strictly to diffusion into a spherical particle, but only a negligible change results when the equations are applied to a cubic geometry (Kondis and Dranoff, 1971). The solution to the Rosen model is given by the following expression:

$$\frac{c}{c_0} = \frac{1}{2} + \frac{2}{\pi}\int_0^\infty \exp\{-\xi_R H_1(\lambda)/5\}$$

$$\times \sin\{2\lambda^2\tau_R/15 - \xi_R H_2(\lambda)/5\}\frac{d\lambda}{\lambda} \qquad (20)$$

where the dimensionless distance is

$$\xi_R = \frac{60D_{micro}Kz\alpha}{(d')^2 v_0} \qquad (21)$$

and the dimensionless time is

$$\tau_R = \left(\frac{60D_{micro}}{(d')^2}\right)\left(\frac{t - \epsilon z}{v_0}\right). \qquad (22)$$

Note that no mass-transfer coefficient appears in this solution, but only the intraparticle diffusion coefficient. This model will be most useful when this intraparticle diffusion is slow. Both models will be useful in analyzing the experiments described next.
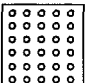
Experimental

Materials

In this work, we measured adsorption of ethane from helium in hollow fiber adsorbers packed with zeolite 4A or zeolite 13X. Two gas mixtures were used, one containing 0.983 vol. % ethane in helium and the other containing pure helium (99.9999%) (Toll Company). The ethane/helium mixture served as the feed during adsorption runs, while the pure helium was used to determine elution curves and to clean the columns between experiments. The zeolite crystals had diameters ranging from 1 to 4 μm for the 4A and 1 to 4.5 μm for the 13X (Union Carbide, lots 941090060030 and 945090001, respectively). The main difference between the zeolites is pore size: 4A has a pore size of about 4 Å while 13X has a pore size of about 10 Å. This difference is reflected in the effective diffusion coefficients of various species in the zeolites: the effective diffusivity of ethane in 4A is between four and eight orders of magnitude smaller than in 13X (Bhatia, 1990; Hyun and Danner, 1985; Antonson and Dranoff, 1969).

Apparatus

We measured breakthrough curves for beds containing a single fiber and for beds containing multiple fibers. The single-fiber beds were made from stainless-steel tubes with a length of 20 cm and outer diameters of 3/16, 1/4, 3/8 and 1/2 in. (4.8, 6.4 and 12.7 mm). A single hollow fiber (Celgard, Hoechst-Celanese, Charlotte, NC) with an inner diameter of 400 μm ran through the center of the tube, while zeolite powder was packed in the shell-side space. The fiber wall contained 20% voids (Celgard X10) or 40% voids (Celgard X20). The zeolite was activated by purging with dry helium at 400°C for 12 h. It was packed into the beds in a glove bag inflated with dry helium.

The several designs used for the multiple fiber beds are summarized in Table 1. The cylindrical multiple-fiber beds (designs 1 and 2) were constructed from glass columns with 1.59 cm OD, approximately 1.07 cm ID, and a total length of approximately 35 cm. A rectangular bed (design 3) was also developed in which the cylindrical glass columns were replaced by a rectangular Plexiglas box. This box had a square cross section with inner dimensions of 1.5 cm × 1.5 cm and a total length of approximately 45 cm. Transparent materials were chosen for column construction because packing deformities were easily visible and hence could be corrected during packing. The first and third designs shown in Table 1 used Celgard type X20 hollow fibers, with inner diameters of either 240 or 400 μm. For the second design, individual fibers were replaced by hollow fiber fabric. This fabric, which has been used previously to recover dissolved oxygen from water (Wickramasinghe et al., 1992), has a warp consisting of Celgard X10 fibers with inner diameters of 240 μm. The fabric has a weft of polyfilament nylon with a total thickness of approximately 30 μm. Activation and packing of the zeolite were done in the same manner as for the single-fiber beds. Additional details for methods of construction for both the

Table 1. Multiple-Fiber Bed Designs

Design No.	Design Description	Column Cross Section
1	Cylindrical column with separated fibers	
2	Cylindrical column with hollow-fiber fabric	
3	Rectangular box with separated fibers	

single-fiber and multiple-fiber columns are given elsewhere (Gilleskie, 1993).

The apparatus used to measure the breakthrough curves is shown in Figure 2. Before entering the hollow fiber column, each gas flowed through a pretreatment column. These columns, which remove impurities like carbon dioxide and water from the feed gas, consisted of 1/2-in. (12.7-mm)-OD steel tubes [ID = 5/16 in. (7.9 mm)] which were packed to a depth of 20 cm with 1/16-in.-dia. (1.6-mm-dia.) zeolite 13X spherical pellets (Alrich, lot number 10415AX). Since the zeolite in the pretreatment columns adsorbs ethane, these columns were saturated with the feed mixture before each experiment to ensure that a constant composition of ethane was entering the hollow fiber bed. Impurities in the gas mixture were more strongly adsorbed onto the zeolite than ethane; thus, they were adsorbed even when the column was saturated with ethane. The impurities in the feed stream were at low levels so that any ethane displaced by the impurities did not significantly alter the composition of the mixture leaving the pretreater.

The disadvantage of using zeolite 13X in the pretreatment column for the feed mixture was the long time often required to saturate the adsorbent with the feed. A more convenient, equally effective pretreater was used in later experiments. This pretreater consisted of two polyvinyl chloride (PVC) columns, each with a 5/8-in. (15.9-mm) OD, packed to a depth of 25 cm, and used in series. The first column was packed with Ascarite (II) (Aldrich, lot number 03612JX), which adsorbs carbon dioxide. The second column was packed with indicating Drierite to remove any moisture. Since neither of
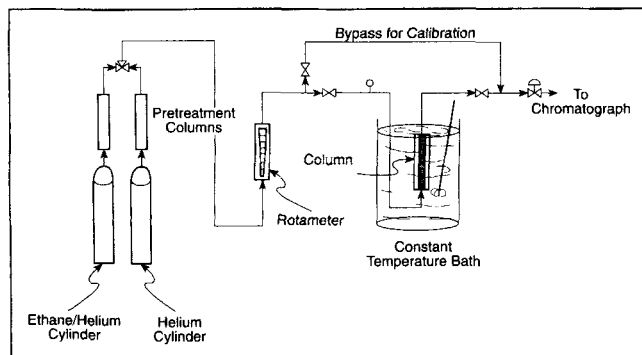
these materials adsorbs ethane, it was not necessary to wait for the columns to become saturated with the feed mixture.

After exiting the pretreater, the feed stream flowed through a Matheson rotameter (type 601) to monitor the feed flow rate. The feed stream pressure, controlled at the gas cylinder regulator, was monitored by a pressure gauge (Ashcroft, type 1009) placed at the bed entrance. A needle valve located at the effluent end of the bed was used to control the flow rate passing through the column. This flow was checked periodically with a soap-film bubble meter. In addition to the needle valve, the system contained two on/off valves situated at each end of the column. They were used to isolate the bed from the rest of the system when necessary. The on/off valve located at the bed entrance was also used to introduce the feed mixture to the column.

The ethane concentration at the column outlet was measured with a Shimadzu GC-15A gas chromatograph equipped with a thermal conductivity detector and run isothermally. The effluent from the bed flowed directly to an automatic sampling valve attached to the gas chromatograph, which contained a Porapak N column (Alltech Associates, Deerfield, IL). The sample loop was calibrated before and after each run with ethane/helium mixtures of known composition. The experimental system also contained a bypass loop through which calibration gases could pass without contacting the hollow fiber column. The loop was removed during experimental runs to minimize the dead volume of the system.

Procedure

Each adsorption experiment was begun with a chromatographic calibration. After the calibration, the system lines were purged with the pure helium. The hollow fiber bed was then filled with pure helium to the pressure at which the experiment was to be run. Following this pressurization, the column was isolated from the system, and the flow lines leading to the column were flushed with the ethane/helium mixture. After flushing, the mixture was switched to the column and the effluent concentration was periodically monitored with the gas chromatograph.

Applying the linear driving force and rosen models

The removal of ethane from helium using zeolite 4A or 13X was not chosen because it is a difficult separation. Rather, it was chosen because it adheres to the assumptions made in developing the theoretical models just developed. Helium was chosen as the carrier gas because it does not adsorb significantly on either zeolite; thus, the gas mixture contained a single dilute adsorbing species, namely ethane. The small amount of ethane present in the mixture means that the velocity of the gas traveling through the hollow fiber bed was approximately constant. The small amount of ethane also means that heat effects were minimized. Most importantly, ethane exhibits a linear isotherm over the range of ethane partial pressures considered (Kondis and Dranoff, 1971; Hyun and Danner, 1982). We validated the linearity of the isotherms by running breakthrough experiments at different pressures and determining the amount of ethane adsorbed at each pressure by mass balance (Gilleskie, 1993).

The experimental breakthrough curves were compared with predictions of the linear driving force and Rosen models ob-

Figure 2. Apparatus used to measure breakthrough curves.

Table 2. Properties of Single-Fiber Beds Used in This Study

Column No.	Column OD in. (cm)	Column ID (cm)	Zeolite Type	Fiber Type	Bed Density (g/cm^3)	α	ϵ	a (cm^2/cm^3)
SF-3/16-1	3/16 (0.48)	0.31	13X	X20	0.60	0.38	0.0167	4.37
SF-1/4-1	1/4 (0.64)	0.46	13X	X20	0.60	0.39	0.0076	1.94
SF-1/4-2	1/4 (0.64)	0.46	4A	X20	0.66	0.41	0.0076	1.83
SF-3/8-1	3/8 (0.95)	0.70	13X	X20	0.60	0.39	0.0033	0.84
SF-3/8-2	3/8 (0.95)	0.70	13X	X10	0.61	0.40	0.0033	0.82
SF-1/2-1	1/2 (1.27)	1.16	13X	X20	0.60	0.39	0.0012	0.30

tained by numerical evaluation of Eqs. 9 and 20 (Gilleskie, 1993). To ensure that accurate solutions were obtained with our numerical procedure, breakthrough curves for a range of parameters were calculated and compared to published results (Furnas, 1930; Rosen, 1954). In all cases, there was good agreement between our solutions and those in the literature.

Calculating solutions to Eqs. 9 and 20 requires estimates of the diffusion coefficient D_{micro}, the overall mass-transfer coefficient k, and other parameters. Values of D_{micro} may be found in the literature (Bhatia, 1990; Hyun and Danner, 1985; Antonson and Dranoff, 1969). Estimates of k require the many parameters given in Eqs. 12–15. The particle diameter d' for each zeolite was taken as 2.5 μm, the arithmetic average of the upper and lower bounds of the particle size reported for 4A. The fraction of volume within the bed available for flow ϵ, and the fraction of column volume that contains zeolite α are given by the following expressions:

$$\epsilon_{cyl} = \frac{n(d)^2}{(d_c)^2} \tag{23}$$

$$\epsilon_{rect} = \frac{n\pi(d)^2}{4(w_{ic})^2} \tag{24}$$

$$\alpha_{cyl} = \frac{4m_{zeolite}/\rho_{zeolite}}{\pi(d_c)^2 L} \tag{25}$$

$$\alpha_{rect} = \frac{m_{zeolite}/\rho_{zeolite}}{(w_{ic})^2 L} \tag{26}$$

where n is the number of fibers in the column, d_c is the inner diameter of the column, $(w_{ic})^2$ is the cross-sectional area of the rectangular column, L is the bed length, $m_{zeolite}$ is the zeolite mass, and $\rho_{zeolite}$ is its density. Equations 23 and 25 apply to cylindrical beds (that is, the single-fiber beds and the cylindrical multiple-fiber beds), while Eqs. 24 and 26

apply to the rectangular multiple-fiber bed. The fiber area per volume of adsorbent a for all columns is calculated from the expression

$$a = \frac{4}{d} \frac{\epsilon}{\alpha}. \tag{27}$$

The actual values of these geometrical quantities of the single-fiber beds are given in Table 2 and for the multiple-fiber beds in Table 3. The gas velocity for each run was determined by dividing the measured volumetric flow rate by cross-sectional area of the fiber and correcting for pressure. Values for the equilibrium constant K were determined for each individual run by a mass balance on the breakthrough curve. Values for these and other operating parameters for each run are shown in Table 4.

Results

This article seeks to compare adsorption in hollow-fiber beds with that in conventional packed beds. Fiber beds potentially have the advantages of low pressure drop, less particle attrition, and more uniform geometry. Fiber beds have the disadvantage of an additional resistance to mass transfer due to the hollow fiber membrane.

Our comparison of hollow-fiber adsorption and packed bed adsorption is simplified by two important features of our experiments. First, we have chosen to study the commercially unimportant separation of ethane adsorbed from helium. We have chosen this system because it has a linear equilibrium isotherm.

The second important feature of our experiments is our choice of two zeolites of different pore size. In one of these zeolites, 4A, the diffusion of ethane is substantially slower than in the other zeolite, 13X. The result is very different adsorption dynamics. In zeolite 4A, the adsorption rates and hence the breakthrough curves are controlled by diffusion within the 2.5-μm zeolite particles. Thus, adsorber dynamics

Table 3. Properties of Multiple-Fiber Beds Used in This Study*

Column No.	Column Design	Packed Length (cm)	No. of Fibers (n)	Fiber Type/ ID (μm)	Bed Density (g/cm^3)	α	ϵ	a cm^2/cm^3
MF-1	1	31.4	21	X20/400	0.57	0.36	0.029	8.21
MF-2	1	30.5	36	X20/240	0.59	0.37	0.018	8.08
MF-3	1	31.5	16	X20/400	0.55	0.35	0.022	6.38
MF-4	1	31.5	16	X20/400	0.57	0.36	0.022	6.15
MF-5	2	30.0	150	X10Fabric/240	0.54	0.31	0.076	40.6
MF-6	3	40.7	121	X20/400	0.57	0.34	0.068	19.9

*All runs used zeolite 13X.

Table 4. Summary of Breakthrough Runs*

Run No.	Column	Velocity (cm/s)	K
1SF	SF-3/8-1	74	490
2SF	SF-3/8-1	162	500
3SF	SF-3/8-1	252	494
4SF	SF-3/8-1	487	493
6SF	SF-3/8-2	164	503
9SF	SF-3/16-1	160	490
11SF	SF-1/4-1	161	494
12SF	SF-1/2-1	163	495
13SF	SF-1/4-2	162	711
1MF	MF-1	163	485
2MF	MF-2	165	482
3MF	MF-3	165	507
4MF	MF-4	168	509
5MF	MF-5	38	492
6MF	MF-6	35	486

*All runs were made at a pressure of 54.7 psia (377 kPa) and a temperature of 23°C.

are not affected by the presence of the fiber wall. In zeolite 13X, the faster micropore diffusion means that adsorption kinetics are controlled by transport outside the particles, and hence may be influenced by the hollow fiber membrane. The performance of the hollow fiber adsorber will be compromised if mass transfer is severely retarded by diffusion across the hollow fiber wall.

Single-fiber beds

First, we compare typical breakthrough curves for the two zeolites in Figure 3. Clearly, the bed packed with 4A produces a more disperse curve than the bed packed with 13X. To illustrate this, let the breakthrough time correspond to the time at which $c = 0.05c_0$. For the bed containing 4A, this time is approximately 5.3 min, while it is 22.5 min for the bed containing 13X. Thus the curve for the zeolite 4A system has a substantially earlier breakthrough time than that for the 13X system, even though 4A adsorbs almost 40% more ethane than 13X at the operating pressure of 54.7 psia (377 kPa).

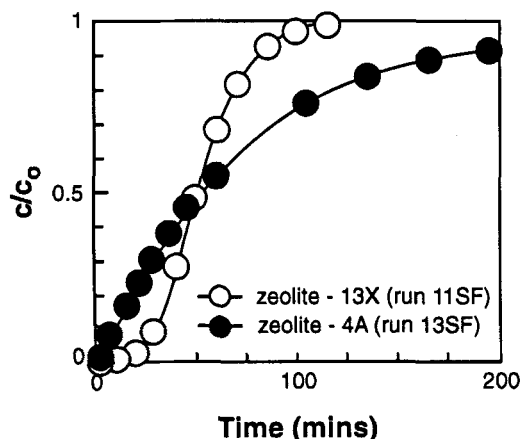The difference between these breakthrough curves reflects

Figure 3. Breakthrough curves for different zeolites.

Ethane diffusion in zeolite 4A (closed points) is much slower than in 13X (open points). This causes the differently shaped breakthrough curves. The solid lines are those estimated from theory (see text).

the very different diffusion coefficients in the two zeolites. The diffusion coefficient of ethane in zeolite 4A is much smaller, equal to 5×10^{-13} cm²/s (Antonson and Dranoff, 1969). As a result, the ratio $4 D_{micro} t / (d')^2$ is much less than 0.1, and the Rosen model for adsorption applies. When we use this model to predict the breakthrough, we get the solid line shown passing through the filled data points in Figure 3. The close agreement between this prediction and the data is strong evidence that diffusion into the zeolite crystal limits the mass-transfer rate; hence, the fiber wall has no effect on the separation.

Although we ran no experiments with other single-fiber columns containing zeolite 4A, we can anticipate the behavior that would result when the inner diameter of columns packed with zeolite 4A is varied. If the inner diameter of the bed is smaller than 0.46 cm (the inner diameter of the 1/4-in. (6.4-mm) column), the zeolite crystals would remain the rate-limiting resistance. If the inner diameter of the column were increased, the wall and macropore contributions to the mass-transfer resistance would become more significant and might begin to affect the overall mass-transfer rate.

We now turn to our more extensive experiments on single-fiber beds packed with zeolite 13X. That our experiments with these beds are more extensive than those with 4A is ironic, for the 13X fiber beds will often be *less* effective than conventional packed beds. Our emphasis reflects our desire to define carefully the limits of hollow-fiber adsorption.

We expect that the dynamics of beds packed with zeolite 13X is unaffected by diffusion inside the zeolite particles, because the diffusion coefficients of ethane in 13X is substantially larger than that in 4A. Reported diffusivities for the ethane/13X system vary. For example, Bhatia (1990) cites a value of 7×10^{-5} cm²/s, while Hyun and Danner (1985) report a measured value of 7.6×10^{-9} cm²/s. Regardless, the diffusivity of ethane in 13X is clearly much greater than that in 4A. Thus we expect that bed dynamics might be affected by the mass transfer in the fiber lumen, by diffusion across the fiber wall, or by diffusion in the macropores between the particles. We explore the effect of each in the following paragraphs.

Figure 4 shows four breakthrough curves measured for column SF-3/8-1 at nominal gas velocities of 500, 250, 160 and 70 cm/s (runs 4SF, 3SF, 2SF, and 1SF in Table 4). Because these velocities correspond to Reynolds numbers of 63, 32, 20, and 9, respectively, the flow is laminar. The points represent actual experimental data; the solid lines are the predictions of the linear driving force model with an overall mass-transfer coefficient equal to 0.0019/s. This value was found to provide the best fit for the data at 160 cm/s. Though the fit at the lowest velocity is slightly poorer, we conclude from these data that the rate constant k does not vary with feed velocity over the range of velocities studied.

We now can use the linear driving force model to help determine which individual mass-transfer coefficients given in Eqs. 12–15 limit the overall rate constant, k, equal to 0.0019/s. For the case in which micropore diffusion limits the separation, the overall mass-transfer coefficient given by Eq. 12 reduces to the term in Eq. 15. With an effective diffusion coefficient equal to 7.6×10^{-9} cm²/s and with a particle diameter equal to 2.5 μm, the mass-transfer coefficient is 7.3/s. This value, much greater than that observed in the experi-
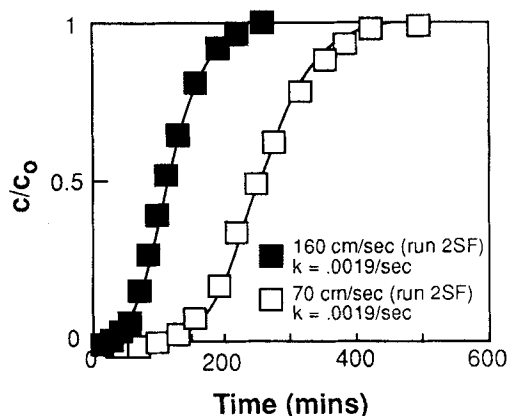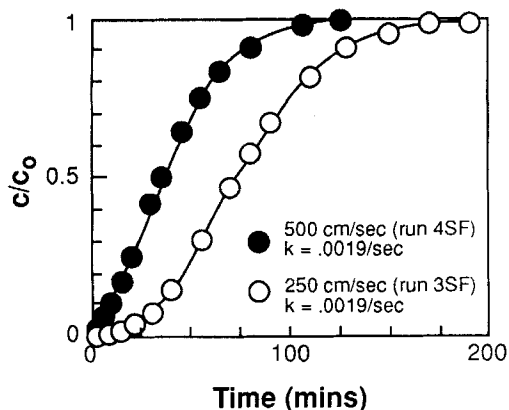
Figure 4. Breakthrough curves at different velocities.

The solid lines are predicted by the linear driving force model with $k = 0.0019/s$.

Figure 5. Predicted breakthrough curves for different mechanisms.

The values of 7.3 and 0.0256/s are expected for micropore control and fiber lumen control, respectively. These values predict sharper breakthrough than is observed.

that in Figure 5 and is represented by the filled squares. The curve for the X10 fiber, which has 20% pores, is represented by the unfilled triangles. The breakthrough curve obtained for the less porous X10 fiber is somewhat more disperse than that obtained from the more porous X20 fiber. These data imply that the wall of the X10 fiber offers a significant resistance to mass transfer.

We can speculate about the extent to which the overall mass resistance depends on the fiber wall by considering the total resistance for both the X10 and X20 beds. The total resistance for each case is the sum of the resistance due to

ments in Figure 4, gives the near vertical breakthrough curve shown in Figure 5. Micropore diffusion cannot explain these data.

We next turn to the case where diffusion within the fiber lumen dominates mass transfer. In this case, k reduces to $k_{lumen} a/K$ with k_{lumen} given by Eq. 13. The diffusion coefficient of ethane in helium can be estimated at 0.14 cm^2/s from the Chapman-Enskog theory (Bird et al., 1960). The fiber has an inner diameter of 0.04 cm, and K is found to be 500; thus, k should equal $0.0256/s$. The breakthrough curve predicted from this value, also shown in Figure 5, is much steeper than that observed experimentally. Like micropore diffusion, mass transfer within the hollow-fiber lumen has little effect on the overall mass-transfer coefficient in a single-fiber adsorbent bed.

We then consider the effect of diffusion across the membrane wall on the overall mass-transfer coefficient k. We could estimate this effect by assuming that k is dominated by k_{wall}, which can be estimated from Eq. 14. Unfortunately, we know neither the diffusion coefficient for ethane through the membrane pores nor the effective thickness of the membrane. Instead, we compare curves from beds containing fibers with different wall porosities in Figure 6. The curve shown for the X20 fiber, which is 40% pores, is the same as
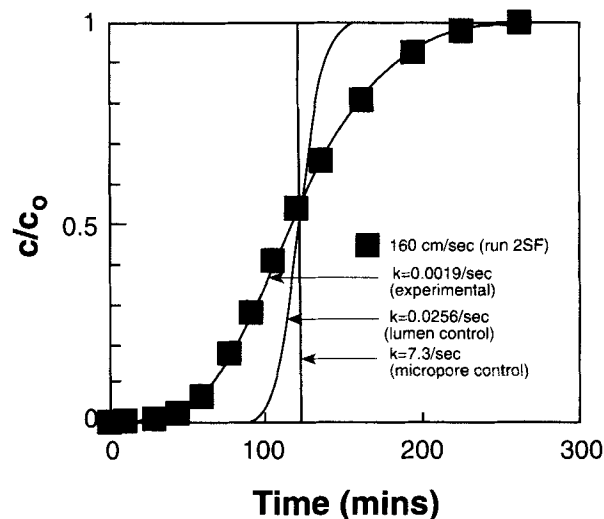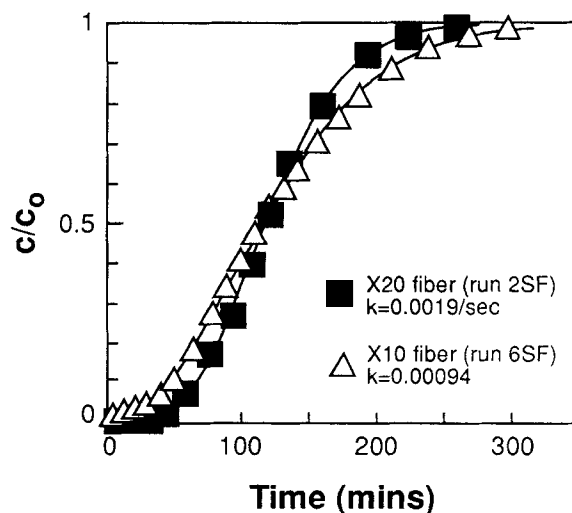

Figure 6. Breakthrough curves for fibers with different wall porosities.

The filled squares are for more porous X20 fiber, and the open triangles are for a less porous X10 fiber. The data imply that resistance to diffusion across the fiber wall is significant.

the fiber wall and the resistance from all other sources. The total resistance to mass transfer is equal to the reciprocal of k for each curve. As noted previously, the X20 curve has a value for k of 0.0119/s. The value for the bed containing the X10 fiber is 0.00094/s. We have measured values for the permeability of nitrogen across the wall of each fiber. Based on these measurements, the ratio of the wall resistances is 3:1. From this ratio and from the values measured for the overall resistance, we infer that the membrane is responsible for about 50% of the mass-transfer resistance in the X20 bed. It is responsible for about 75% of the resistance in the X10 bed.

Finally, we turn to the effect of mass transfer in the spaces between the zeolite particles, the macropores. As mentioned in the Theory section, we know of no way to estimate this effect *a priori*. Instead, we studied it by measuring breakthrough curves in beds with a single hollow fiber of fixed diameter but with different column diameters and hence different depths of zeolite particles. Our results, given in Figure 7, show the experimental breakthrough curves obtained with four different columns: SF-3/16-1 (run 9SF), SF-1/4-1 (run 11SF), SF-3/8-1 (run 2SF), and SF-1/2-1 (run 12SF). Each curve was measured at identical experimental conditions. Figure 7 also gives predictions of the linear driving force model. The mass-transfer coefficients used to generate these
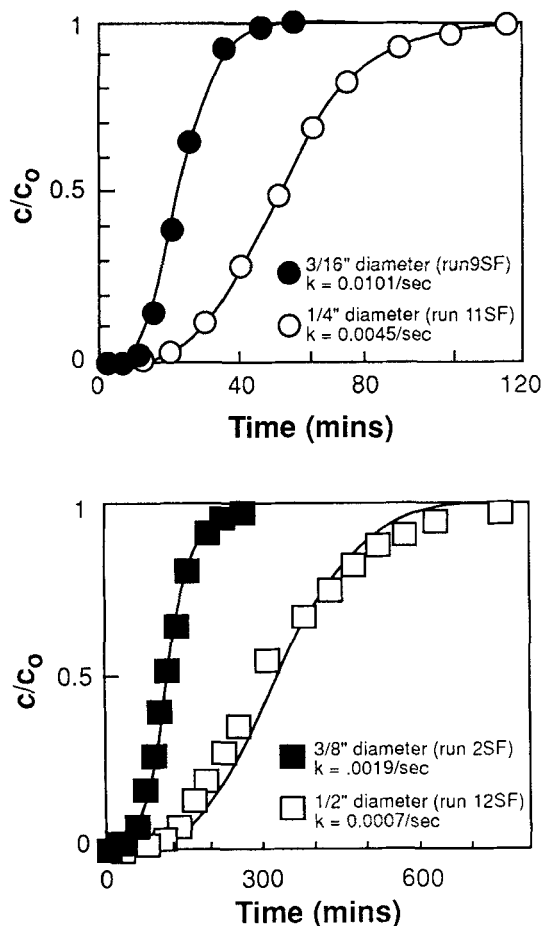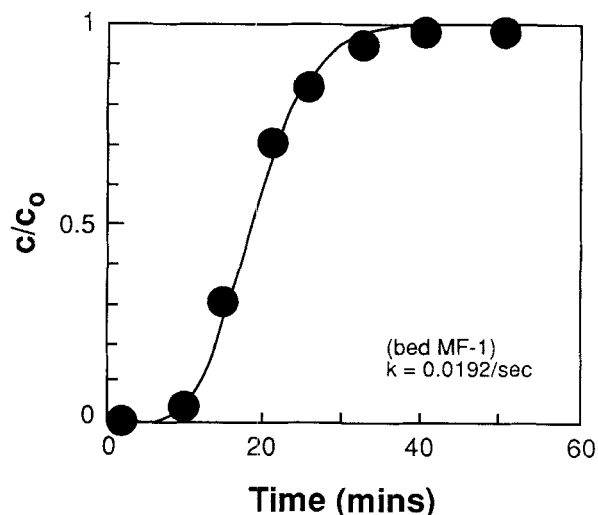

Figure 8. Breakthrough curve for a bed with twenty-one evenly spaced fibers.

The solid curve is a prediction from measurements on single-fiber beds.

curves were calculated by assuming that the fiber wall provides all of the resistance to mass transfer within the bed; under this assumption, the overall mass-transfer coefficient is equal to $k_{wall}\, a/K$. To determine the appropriate value of k for each column, k_{wall} was calculated from the best-fit coefficient from run 2SF. Note that since the quantity of zeolite in each column increases as the inner diameter increases, the values of a and hence of k decrease with increasing column diameter. Interestingly, these mass-transfer coefficients provide excellent fits for the SF-3/16-1 and SF-1/4-1 beds. The agreement between the theoretical and experimental curves indicates that the fiber wall significantly limits mass-transfer rates in these beds. The curve measured for the 1/2-in. (12.7-mm) bed, however, is broader than the curve predicted by assuming that only the wall resistance is important. This result indicates that as the depth of packing is increased, the macropore resistance becomes increasingly important.

Multiple-fiber beds

We next extend our analysis of adsorption in single-fiber beds containing zeolite 13X to multiple-fiber beds containing the same zeolite. To make this extension, we hypothesize that the annular cylindrical geometry of the single-fiber beds, with mass transfer across the fiber wall and an impermeable boundary at the bed's outer surface, can approximate one fiber and its surrounding absorbent in a multiple-fiber bed.

One experiment testing this hypothesis is shown in Figure 8. This curve was measured at the same experimental conditions used to obtain the curves in Figure 7. Recall that the mass-transfer coefficients used to obtain the theoretical curves in that figure were determined by setting $k = k_{wall}\, a/K$, where k_{wall} was obtained from the best-fit mass-transfer coefficient for run 2SF. The coefficient k inferred for bed MF-1 in the identical manner is 0.0192/s. The resulting prediction, given by the solid line in Figure 8, matches the experiment well.

The agreement between theory and experiment in Figure 8

Figure 7. Breakthrough curves for beds of varying diameter.

These data, all for a single hollow fiber of fixed wall porosity, show that wall resistance is important.

is important for three reasons. First, it indicates that the difference in the geometry of diffusion between the multiple- and single-fiber beds has little effect on the breakthrough curve. Second, the agreement shows that the difference in length between the single-fiber beds (20 cm) and this multiple-fiber bed (31.5 cm) also has no significant effect on the breakthrough curve. Third and most importantly, these data demonstrate that larger beds can be constructed that are relatively free of dispersion. Dispersion in multiple-fiber beds may be important when there are variations in the physical dimensions of individual fibers within a bed (for example, inner diameter or porosity), or when the quantity of solid packed around different fibers varies. When such variations exist, fluid streams passing through different fibers will be exposed to different conditions. When the streams combine at the bed outlet, the net effect will be a breakthrough curve that is broader than the curve that would result if each individual stream saw exactly the same conditions.

The agreement between theory and experiment in Figure 8 was obtained only after a series of refinements in the method for constructing columns. Many beds constructed during this research gave breakthrough curves that did not match the predictions generated from the mass-transfer coefficients of the single-fiber data. As an example, we consider the data shown in Figure 9, obtained from a bed that contained 36 fibers with inner diameters of 240-μm. The value of k expected for this case from the single-fiber data is 0.0190/s. The curve generated by the linear driving force model with this value does not fit the data, as shown in the figure. A curve generated with $k = 0.0095$/s, a mass-transfer coefficient one-half the predicted value, agrees much more closely with the experiment.

We are not sure whether the greater dispersion of the data in Figure 9 is due to unequal fiber diameters, unequal wall porosities, or to uneven zeolite packing. We do know that the 240-μm fibers used to construct bed MF-2 are less permeable than the 400-μm fibers used in the single-fiber measurements. Although both the 240- and 400-μm fibers are said by the manufacturer to be the same type (X20), our measurements of the flux of nitrogen across the walls of our fibers at a transmembrane pressure difference of 5 psia indicate that the permeability of the 240-μm fiber is about three-quarters that of the 400-μm fiber. Since the fiber wall offers a significant resistance to mass transfer, the difference in permeability between the fibers contributes to a more disperse breakthrough curve.

We also know that one of the most challenging aspects of column construction is keeping fibers evenly spaced during packing. Uneven fiber spacing leads to unequal amounts of zeolite surrounding each fiber; hence, different fibers may have different adsorption capacities. To study the effect of nonuniform fiber packing, we built two beds, denoted in Table 3 as MF-3 and MF-4. Each bed has exactly the same dimensions and the same number of fibers; the only difference is that the fibers in MF-3 are distributed evenly throughout the column volume, while the MF-4 fibers are potted through the center of the column. As shown in Figure 10, the resulting breakthrough curve from the bed with the fibers potted through the center is broader than the curve obtained from the bed with evenly distributed fibers. While these two cases represent extremes, we expect that a family of curves lying
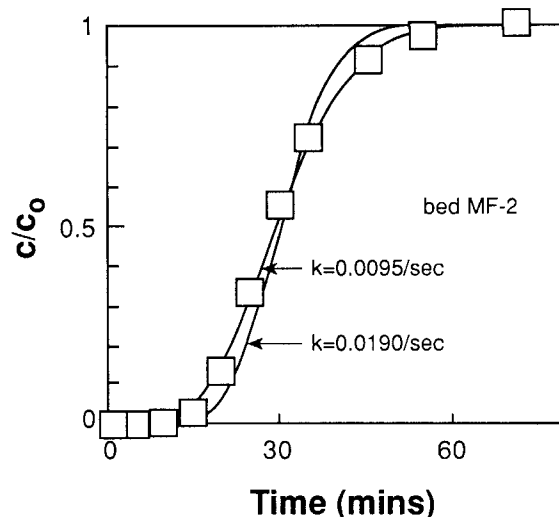

Figure 9. Breakthrough curve for a bed with thirty-six fibers.

The rate constant of 0.0095/s which fits these data is about half the value expected from single-fiber experiments. Behavior like this is characteristic of all but very carefully constructed beds.

between those shown in Figure 10 could be generated by varying the spacing of the fibers.

To better understand the column dynamics of the unevenly spaced bed MF-4, we consider the idealized case in which none of the ethane is adsorbed from the gas flowing through the two of the inner fibers, which are imagined to have no adsorbent surrounding them. If all of the ethane flowing through the remaining fourteen fibers is adsorbed during the first several seconds of the breakthrough run, then the value of c/c_0 immediately after the void volume has been cleared ($L/v = 0.19$ s) would equal 2/16 or 0.125. The first data point
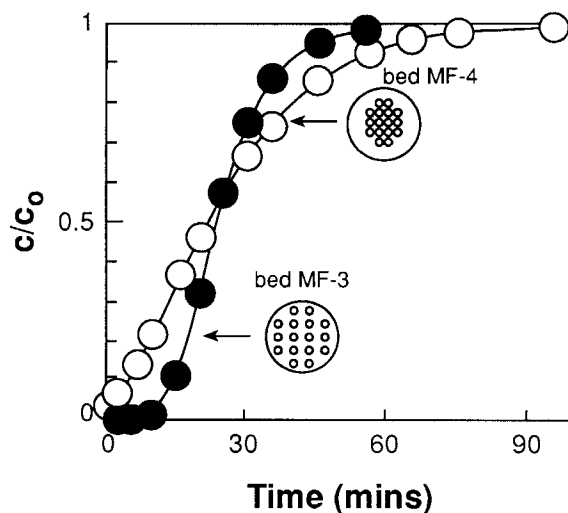

Figure 10. Breakthrough curves for different hollow fiber spacing.

Uneven spacing, like that in bed MF-4, results in a more disperse breakthrough curve than for the evenly spaced bed MF-3.
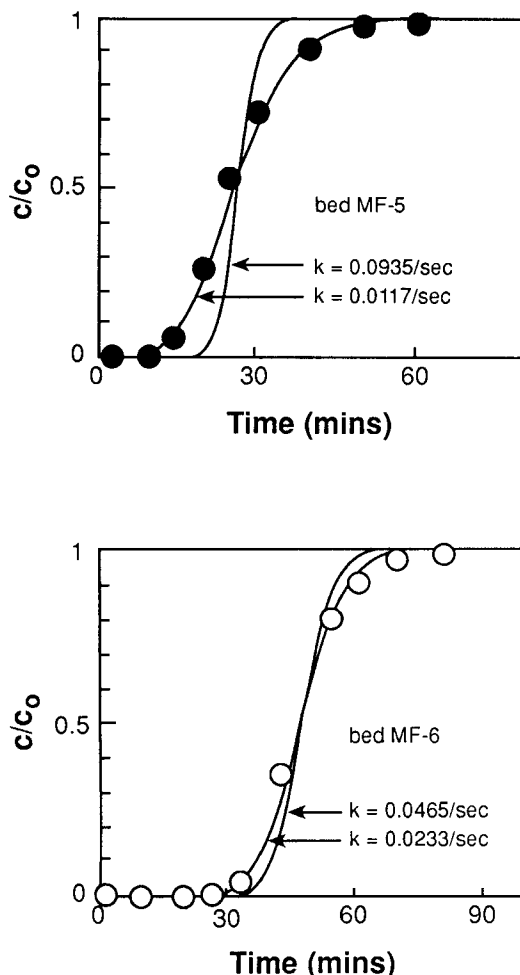
Figure 11. Breakthrough curves for beds with larger fiber area per bed volume.

The rate constants inferred from the data (0.0117 and 0.0233/s) are less than those expected from single-fiber experiments (0.0935 and 0.0465/s).

on the MF-4 curve in Figure 10 was taken at one minute, at which time $c/c_0 = 0.028$. This value is significantly smaller than that predicted. Hence some adsorption still occurs from each fiber. If it did not, the breakthrough curve would be even broader than that measured.

Thus far, our discussion of multiple-fiber beds has been limited to beds of the first design listed in Table 1. These beds, made with 2.5-μm zeolite crystals, have a fiber area per bed volume of around 3 cm^2/cm^3. In contrast, a conventional bed with 1,600 μm (1/16-in.) zeolite pellets and a void fraction of 0.4 has a particle area per bed volume of around 20 cm^2/cm^3. Thus a conventional bed limited by macropore diffusion has around seven times more area for mass transfer than our hollow fiber beds.

We attempted to increase the surface area for mass transfer within the multiple-fiber adsorbers by using the second and third designs listed in Table 1. The values of the bed density for MF-5 (design 2) and MF-6 (design 3) are close to those obtained in the single-fiber beds, while the membrane area per unit volume of zeolite is larger, as shown in Table 3. Unfortunately, the breakthrough curves for these designs are

broader than those inferred from the single-fiber data, as shown by Figure 11.

There are several causes for these compromised separations. Bed MF-5 was constructed with hollow fiber fabric of the type X10 fiber, which has a nominal porosity of 20%. Since the fiber wall offers a significant resistance to mass transfer in this bed, we expect that the mass-transfer coefficient should be smaller than that predicted from the single-fiber data, which used X20 fibers with a nominal porosity of 40%. This correction is not enough to explain the results, however, for the coefficient predicted is nearly an order of magnitude too large. Thus the additional dispersion in Figure 11 must be largely due to uneven fiber spacing.

Discussion

A major goal of this research is to compare the performance of hollow fiber adsorbers with that of conventional packed bed adsorbers. Our experiments to date show that the particular beds that we have used can be significantly improved. If we were to continue our development of the hollow fiber absorbers, we would make several changes. We would use hollow fibers with higher porosity, larger pores, and thinner walls to reduce resistance to mass transfer across the fiber wall. We would continue to explore ways to space the hollow fibers evenly; for example, we have discussed giving them a static electric charge, so that they would position themselves during module construction.

Still, we know enough about these multiple fiber beds to compare their best possible performance with conventional packed beds. We do so by means of specific examples. These examples are based on the physical properties in Table 5 for two fiber beds and two conventional beds. The first fiber bed, described in the second column of the table, is based on values typical of our experiments. The second fiber bed, described in the third column, is the best that we think could be made. It would have fibers whose walls offer no resistance to mass transfer; it would have evenly spaced fibers separated with a square symmetry by distances that are exactly twice the diameter of the fiber.

The two conventional beds shown in Table 5 imitate many of the properties of the hollow fiber beds. The real difference comes from the pressure drop Δp involved. For a fiber bed, the pressure drop is given by Eq. 1, while for a conventional bed, the pressure drop is given by Eq. 2. Because we want to operate the beds at equal pressure drop, we see that

$$\frac{vL}{d^2} = \left(\frac{150}{32}\right)\left(\frac{1-\epsilon'}{\epsilon'}\right)^2 \frac{v'L'}{(d')^2}. \tag{28}$$

Thus we cannot choose v, L, and d equal to v', L', and d', respectively. The two conventional beds in Table 5 represent two compromises drawn from Eq. 28. The first, in the fourth column of the table, achieves equal pressure drop with slower velocity. The second in the last column of the table, achieves equal pressure drop with larger particles.

To compare these beds, we recognize that the bed productivity is proportional to the rate of feed times the fraction of bed saturated. The feed rate is proportional to the superficial velocity and so is known from the values in Table 5. Because

Table 5. A Comparison of Hollow Fiber and Conventional Adsorption Beds*

Properties	Current Fiber Bed	Improved Fiber Bed[†]	Conventional Bed—Small Particles[‡]	Conventional Bed—Large Particle[§]
Crystal size, μm	2.5	2.5	2.5	2.5
Particle size, μm	2.5	2.5	400	1,300
Fiber dia., μm	400	400	—	—
Vol. for flow/vol. bed ϵ	0.03	0.20	0.40	0.40
Vol. Crystals/vol, bed α	0.36	0.36[‖]	0.35	0.35
Bed length, m	1	1	1	1
Actual vel., m/s	2.5	2.5	0.24	2.5
13X-Mass Transfer				
Outside Crystals Controls				
Rate constant, k, s^{-1}	0.019	0.25[#]	2.30**	0.22**
Fraction bed saturated θ	0.74	0.81	∼1	0.72
Relative productivity	1	8	2	14
4A-Mass Transfer				
Inside Crystals Controls				
Relative Productivity	1	∼1	∼1	∼1

*Values in this table come from our experiments except as noted. The equilibrium constant, K, defined as moles adsorbed by a unit crystal volume per moles in a unit gas volume, is taken as 500 for zeolite 13X and 700 for zeolite 4A. These values are close to those we measured experimentally for ethane adsorbed from helium.
**Estimated by assuming that the macropore resistance limits mass transfer in these beds.
[†]Assuming fibers are equally spaced 800 μm apart, with square symmetry.
[‡]Assumes d' equals d and that bed length and pressure drop are the same as the fiber beds, so a smaller velocity.
[§]Has same velocity, bed length, and pressure drop as fiber beds, so a larger particle size.
[‖]Assumed equal to the value for the current fiber bed.
[#]Increased two times by no membrane resistance and approximately seven times by a larger value for a.

no bed's mass transfer is instantaneous, however, faster feeds tend to result in a smaller fraction saturated.

Thus to compare these beds, we must presume a mass-transfer coefficient and hence a mass-transfer mechanism. There are two possible limiting mechanisms. In the first, mass transfer is controlled by diffusion outside the crystals. This limit is true for ethane adsorption on zeolite 13X, and so that is emphasized in this article. When analyzed with the linear driving force model, the limit leads to the productivities shown in Table 5. For convenience, these productivities are defined relative to the current fiber bed.

The results show that an improved fiber bed would outperform the current bed by a factor of 8. Most of this improvement comes from a higher void fraction ϵ, which allows a much larger superficial velocity and also gives a larger fiber area per zeolite volume. Reducing the mass-transfer resistance in the fiber wall is also beneficial, but somewhat to our surprise, has a much smaller effect.

The results in Table 5, however, also show that even the improved fiber bed would not outperform every conventional bed. To be sure, the improved fiber bed would be about four times better than a conventional bed operated at low flow to get a low pressure drop. This improved performance is due to the higher flow in the fibers, and is in spite of the smaller k in the fibers. On the other hand, the improved fiber bed gives inferior performance relative to conventional beds running at the same velocity. If the mass transfer is controlled by diffusion outside the crystals, the best fiber beds would seem to offer similar performance to conventional beds, but would be harder to build.

If mass transfer is controlled by diffusion within the crystals, as with ethane adsorption on zeolite 4A, we find that each bed gives nearly the same performance. Again the relative productivity is proportional to the superficial velocity

times the fraction of bed saturated and was determined from the Rosen model.

Thus we do not anticipate substantially better productivity for adsorption carried out in beds of very small particles and containing hollow fibers. We find that the advantage of the smaller pressure drop possible with hollow fibers is not enough to overcome the disadvantage of a small void fraction available for flow. Interestingly, the mass-transfer resistance in the hollow fiber wall, which is significant in our experiments, is not a major factor in our conclusion.

Conclusions

We have measured ethane adsorption from helium in fixed beds consisting of microporous hollow fibers that span a column packed with a 2.5-μm-dia. zeolite crystals. Our experiments with beds containing only a single hollow fiber and packed with zeolite 4A resulted in breakthrough curves that could be predicted with the Rosen model, indicating that mass transfer is dominated by slow diffusion within the micropores of the zeolite crystals. Our results from experiments with beds containing a single hollow fiber and packed with zeolite 13X show breakthrough curves that can be described by the linear driving-force model. These latter curves are influenced by diffusion across the fiber wall and within the macropores between zeolite crystals.

Our results from beds containing multiple hollow fibers show that the adsorption of ethane onto zeolite 13X crystals can be successfully predicted from mass-transfer coefficients measured from single-fiber beds. However, prediction of the breakthrough curves from multiple-fiber beds is successful only when the fibers are evenly spaced.

A comparison between hollow fiber beds and conventional beds shows that in terms of productivity, a fiber bed would

not always outperform conventional beds, regardless of adsorbent. In multiple-fiber beds containing zeolite 13X, the advantage of the smaller pressure drop possible with the hollow fibers is not enough to overcome the disadvantage of a small void fraction available for flow. Moreover, achieving hollow fiber performance even equal to good conventional beds requires improving module construction beyond that which we found possible. Any decision to use hollow-fiber beds for adsorption must be dominated by factors other than productivity, such as particle attrition.

Acknowledgments

Notation

c_0 = solute concentration in gas phase at bed entrance
$H_1 = \lambda [\sinh(2\lambda) + \sin(2\lambda)]/[\cosh(2\lambda) - \cos(2\lambda)] - 1$
$H_2 = \lambda [\sinh(2\lambda) + \sin(2\lambda)]/[\cosh(2\lambda) - \cos(2\lambda)]$
r = radial coordinate for zeolite crystal
t = time
u = integration variable in linear driving-force solution
z = distance measured from bed inlet
ϵ' = void fraction available for flow in a conventional bed
λ = integration variable in the Rosen solution

Literature Cited

Antonson, R. C., and J. S. Dranoff, "Adsorption of Ethane on Type 4A and 5A Molecular Sieve Particles," *AIChE Symp. Ser.*, **65**, 27 (1969).

Anzelius, A., "Uber Erwarmung Vermittels durchstroemender Medien," *Z. Angew. Math. Mech.*, **6**, 291 (1926).

Bhatia, S., *Zeolite Catalysis: Principles and Applications*, CRC Press, Boca Raton (1990).

Bird, R. B., W. E. Stewart, and E. M. Lightfoot, *Transport Phenomena*, Wiley, New York, (1960).

Carslaw, H. S., and J. C. Jaeger, *Conduction of Heat in Solids*, Oxford Univ. Press, Oxford (1947).

Degen, P. J., and T. C. Gsell, "Self-Supporting Structures Containing Immobilized Carbon Particles and Method for Forming Same," U.S. Patent 4,664,683 (1987a).

Degen, P. J., and T. C. Gsell, "Self-Supporting Structures Containing Immobilized Inorganic Sorbent Particles and Method for Forming Same," U.S. Patent 4,665,050 (1987b).

Furnas, C. C., "Heat Transfer from Gas to Solids," *Trans. AIChE*, **24**, 142 (1930).

Garg, D. R., and D. M. Ruthven, "Theoretical Prediction of Breakthrough Curves for Molecular Sieve Adsorption Columns: I. Asymptotic Solutions," *Chem. Eng. Sci.*, **28**, 791 (1973).

Gibbs, S. L., and E. N. Lightfoot, "Sealing-Up Gradient Elution Chromatography," *IEC Funds.*, **25**, 490 (1986).

Gilleskie, G. L., "Gas Separations in Fixed-Bed Hollow Fiber Adsorbers," PhD Thesis, Univ. of Minnesota, Minneapolis (1993).

Glueckauf, E., "Theory of Chromatography. Part 10. Formulae for Diffusion Into Spheres and Their Application to Chromatography," *Trans. Faraday Soc.*, **51**, 1540 (1955).

Hyun, S. H., and R. P. Danner, "Adsorption Equilibrium Constants and Intraparticle Diffusivities in Molecular Sieves by Tracer-Pulse Chromatography," *AIChE J.*, **31**, 1077 (1985).

Hyun, S. H., and R. P. Danner, "Determination of Gas Adsorption Equilibria by the Concentration-Pulse Technique," *AIChE Symp. Ser.*, **78**, 19 (1982).

Kondis, E. F., and J. S. Dranoff, "Kinetics of Isothermal Sorption of Ethane on 4A Molecular Sieve Pellets," *Ind. Eng. Chem. Process Des. Dev.*, **10**, 108 (1971).

McMinis, C. W., and C. Y. Pan, "Hollow Fiber Bundle Element," U.S. Patent 5,139,668 (1992).

Miller, J. D., and M. G. Verrando, "Sorbing Apparatus," U.S. Patent 4,687,573 (1987).

Newman, J., "Extension of the Leveque Solution," *J. Heat Transfer*, **91**, 177 (1969).

Qi, Z., and E. L. Cussler, "Microporous Hollow Fibers for Gas Adsorption: II. Mass Transfer Across the Membrane," *J. Memb. Sci.*, **23**, 333 (1985).

Rosen, J. B., "Kinetics of a Fixed-Bed System for Solid Diffusion Into Spherical Particles," *J. Chem. Phys.*, **20**, 387 (1952).

Rosen, J. B., "General Numerical Solution for Solid Diffusion in Fixed Beds," *Ind. Eng. Chem.*, **46**, 1590 (1954).

Ruthven, D. M., *Principles of Adsorption and Adsorption Processes*, Wiley, New York (1984).

Sartory, W. K., "Adsorption on the Walls of a Cylindrical Channel," *Ind. Eng. Chem. Fund.*, **17**, 97 (1978).

Tereck, C. D., D. S. Kovach, and M. D. LeVan, "Constant-Pattern Behavior for Adsorption on the Wall of a Cylindrical Channel," *Ind. Eng. Chem. Res.*, **26**, 1222 (1987).

Turnock, P. H., and R. H. Kadlec, "Separation of Nitrogen and Methane via Periodic Adsorption," *AIChE J.*, **17**, 335 (1971).

White, D. H., and P. G. Barkley, "The Design of Pressure Swing Adsorption Systems," *Chem. Eng. Prog.*, **85**, 25 (1989).

Wickramasinghe, S. R., M. J. Semmens, and E. L. Cussler, "Hollow Fiber Modules Made With Hollow Fiber Fabric," *J. Mem. Sci.*, **84**, 1 (1993).